ISSN 0023-1584, Kinetics and Catalysis, 2012, Vol. 53, No. 1, pp. 137–144. © Pleiades Publishing, Ltd., 2012.
Original Russian Text © R.A. Shutilov, I.V. Grenev, O.V. Kikhtyanin, V.Yu. Gavrilov, 2012, published in Kinetika i Kataliz, 2012, Vol. 53, No. 1, pp. 141–149.

# Adsorption of Molecular Hydrogen on Aluminophosphate Zeolites at 77 K

**R. A. Shutilov, I. V. Grenev, O. V. Kikhtyanin, and V. Yu. Gavrilov**

*Boreskov Institute of Catalysis, Siberian Branch, Russian Academy of Sciences, Novosibirsk, 630090 Russia*

*e-mail: gavrilov@catalysis.ru*

Received April 21, 2011

**Abstract**—The $H_2$ sorption properties of the aluminophosphate zeolites AlPO-5, AlPO-31, AlPO-11, AlPO-36, and AlPO-8 at 77 K have been investigated. A series of $H_2$ adsorption isotherms has been obtained for cylindrical micropore channels in the aluminophosphate zeolites. The absolute values of the amount adsorbed $\alpha(P)$ for the mesoporous aluminophosphate materials and the effective density of adsorbed $H_2$ in the micropore space $\beta^*(P, d)$ have been determined. It has been demonstrated experimentally that the sorbate density depends on the size of the micropore channel of the zeolite $d$. Hydrogen sorption isotherms have been calculated from experimental isotherms. A procedure allowing $\beta^*(P, d)$ to be estimated for intermediate $d$ values is presented.

**DOI:** 10.1134/S0023158412010119

Zeolite-containing catalysts are widely employed in various catalytic processes. Noteworthy ones are CuZSM-5 catalysts, which are used in the decomposition of NO [1, 2] and $N_2O$ [3] to $N_2$ and $O_2$, in the selective reduction of $NO_x$ with hydrocarbons [4–6], in ethylene aromatization [7], and in other applications. Along with aluminosilicate zeolites, aluminophosphate (AlPO) zeolites have also found wide use, including in ethylene oligomerization [8], *n*-butene isomerization [9], and $N_2O$ decomposition [10].

An important characteristic of zeolite-containing catalysts is the location of catalytically active association species, clusters, and isolated ions of metals in the pore space of the support. Of significance are both active component distribution in the mesopore space (i.e., on the surface of zeolite crystallites) and active component distribution in the micropore channel space. These active component distributions are a considerable factor in the catalytic and service characteristics of zeolite-containing catalysts [11, 12]. It is, therefore, a challenging problem to advance methods for analyzing the active component distribution in the pore space of a support.

The most widespread method of investigating the active component distribution in the pore space of a support is based on sorption, which typically employs nitrogen at 77 K as the sorbate. Methods for calculating the mesopore size distribution and, accordingly, the modification-induced changes in this distribution have been sufficiently perfected to date. These are mainly continual methods, among which note the classical methods of Barrett, Joyner, and Halenda [13]; Dollimore and Heal [14]; Broekhoff and de Boer [15]; and Horvath and Kavazoe [16]. In recent years, there has been a tendency to improving pore size distribution calculation methods. These improvements have been based on precise molecular calculations using Monte Carlo and molecular dynamic numerical methods and nonlocal density functional theory (NLDFT) [17–19].

The study of micropore ($d < 1.5$–2 nm pore) volume distribution over pore size has been advanced by wide use of DFT. However, at present this method is strictly used only for homogeneous surfaces, for example, carbon surfaces and at least homothetic ones. When extending the NLDFT approach to microporous oxide materials, including zeolites, and, more specifically, when calculating a set of local adsorption isotherms for a particular model and pore size, one faces serious methodological difficulties that are sometimes cannot be circumvented.

Sorbate selection is an important step in micropore structure investigation. Use of the conventional sorbates, namely nitrogen vapor at 77 K and argon vapor at 87 K, for this purpose does not rule out activated diffusion of sorbate molecules in the fine pore space [20, 21]. In practice, a sharp decrees in the rate at which the sorption equilibrium is reached leads to obtaining unreliable experimental data. The problem of activated diffusion can be solved in two ways. The first is to use of sorbates with a smaller kinetic diameter of a molecule, such as molecular hydrogen (0.289 nm), in place of molecular nitrogen (0.364 nm) [22, 23]. The second approach is to carry out a sorption experiment at a higher temperature, for example, $CO_2$ adsorption at 195 K [24]. This would increase the kinetic energy of sorbate molecules and facilitate dif-

**Table 1.** Stock composition and hydrothermal synthesis conditions for aluminophosphates

| Source of aluminum | Stock composition, mol | $T$, °C | Reaction time, h | Product |
|---|---|---|---|---|
| PB | $1Al_2O_3$:$1P_2O_5$:1DPrA:40 $H_2O$ | 180 | 48 | AlPO-11 |
| PB | $1Al_2O_3$:$1P_2O_5$:1DBuA:40 $H_2O$ | 140 | 24 | AlPO-8 |
| AIP | $1Al_2O_3$:$1P_2O_5$:1DBuA:40 $H_2O$ | 180 | 48 | AlPO-31 |
| PB | $1Al_2O_3$:$1P_2O_5$:1TEA:40 $H_2O$ | 200 | 24 | AlPO-5 |
| PB | $1Al_2O_3$:$1P_2O_5$:1.7TPA:40 $H_2O$ | 150 | 192 | AlPO-36 |
| $Al(NO_3)_3$ | $1.2Al_2O_3$:$1P_2O_5$:0.5DPrA:40 $H_2O$ | 200 | 48 | $AlPO_4$-q |
| $Al(NO_3)_3$ | $1Al_2O_3$:$1P_2O_5$:1TPA:40 $H_2O$ | 200 | 48 | $AlPO_4$-c |
| $Al(NO_3)_3$ | $1Al_2O_3$:$1P_2O_5$:40$H_2O$ | 200 | 48 | $AlPO_4$-tr |

fusion in the fine pore space, but it would decrease the measured equilibrium amount adsorbed.

New opportunities in micropore structure analysis are expected from the adsorption of gases, i.e., sorbates above their critical temperature [25]. At these temperatures, there can be no spontaneous micropore volume filling with a liquid-like sorbate and the variation of the sorbate density with an increasing pressure is determined to a considerable extent by the micropore size. This specific feature of the adsorption process may be favorable for determination of textural characteristics of the microporous structure, including calculation of micropore volume distribution of over pore size. Hydrogen adsorption at 77 K satisfies this condition, because, for $H_2$, $T_{cr} = 33.2$ K.

Aluminophosphate zeolites are convenient objects allowing one to vary parameters of the microporous structure, including the size and volume of cylindrical channels accessible to the sorbate molecules [26]. By introducing some cations, e.g., Si into a zeolite, it is possible to further change its structure. The morphological diversity of AlPO materials, with their composition being constant, makes them usable in the investigation of the effect of the size of the cylindrical micropore channel on, e.g., the variation of the density of adsorbed $H_2$ molecules with an increasing equilibrium pressure.

Here, we report the $H_2$ adsorption properties of the mesopores of aluminophosphate materials at 77 K and the correlation between the density of adsorbed $H_2$ in micropore channels of AlPO zeolites and the channel size.

## EXPERIMENTAL

Microporous aluminophosphates were synthesized by the method described in [27, 28]. The source of aluminum was hydrated aluminum oxide (pseudoboehmite, PB, 74.8% $Al_2O_3$, Sasol) or aluminum isopropoxide (AIP, 98%, Aldrich). The source of phosphorus was orthophosphoric acid (76% $P_2O_5$, Reakhim). The structure-forming compounds were di-*n*-propylamine (DPrA, 99%, Aldrich), di-*n*-butylamine (DBuA, 99%, Aldrich), triethylamine (TEA, 97%, Aldrich), and tri-*n*-propylamine (TPA, 99%, Aldrich). Mesoporous aluminophosphates of the same chemical composition were also prepared, which had the close-packing structure of α-quartz (berlinite, $AlPO_4$-q), cristobalite ($AlPO_4$-c), or tridymite ($AlPO_4$-tr). In the synthesis of these materials, the source of aluminum was aluminum nitrate (Acros). The composition of the stocks for aluminophosphate synthesis and the hydrothermal treatment conditions are specified in Table 1. The products of hydrothermal synthesis were washed with distilled water to remove the mother solution, were dried in air, and were calcined at 600–620°C for 3 h.

The objects of this study were synthesized aluminophosphate zeolites AlPO-5 (IUPAC code AFI, unit cell composition $Al_{12}P_{12}O_{48}$), AlPO-11 (IUPAC code AEL, unit cell composition $Al_{20}P_{20}O_{80}$), AlPO-8 (IUPAC code AET, unit cell composition $Al_{36}P_{36}O_{144}$), AlPO-31 (IUPAC code ATO, unit cell composition $Al_{18}P_{18}O_{72}$, and AlPO-36 (IUPAC code ATS, unit cell composition $Al_{12}P_{12}O_{48}$). We also studied the adsorption properties of the mesoporous crystalline aluminophosphates $AlPO_4$-c, $AlPO_4$-q, and $AlPO_4$-tr, which had the same elemental composition as the zeolites, but did not contain micropores.

The X-ray diffraction patterns of the AlPO zeolites were obtained on an ARL X'TRA diffractometer using monochromated Cu$K_\alpha$ radiation (point scanning mode, $2\theta = 5°$–$40°$ , 0.05° increments, counting time of 3 s per point). Unit cell parameters were derived from the main reflections by least squares using the POLIKRISTALL program [29]. The error of determination of unit cell parameters was ±0.003 Å.

Nitrogen and hydrogen adsorption isotherms at 77 K for the aluminophosphate materials in a wide pressure range of 0.01–760 Torr were obtained on a DigiSorb-2600 automated volumetric device (Micromeritics, United States). In order to eliminate the texture irreproducibility effect, the $N_2$ and $H_2$ sorption isotherms were measured for the same sample. All samples were pre-heat-treated in vacuum (350°C, residual pressure of $10^{-4}$ Torr) for 5 h. This allowed all sorbed impurities to be removed. The mesopore volume distribution over pore size was cal-

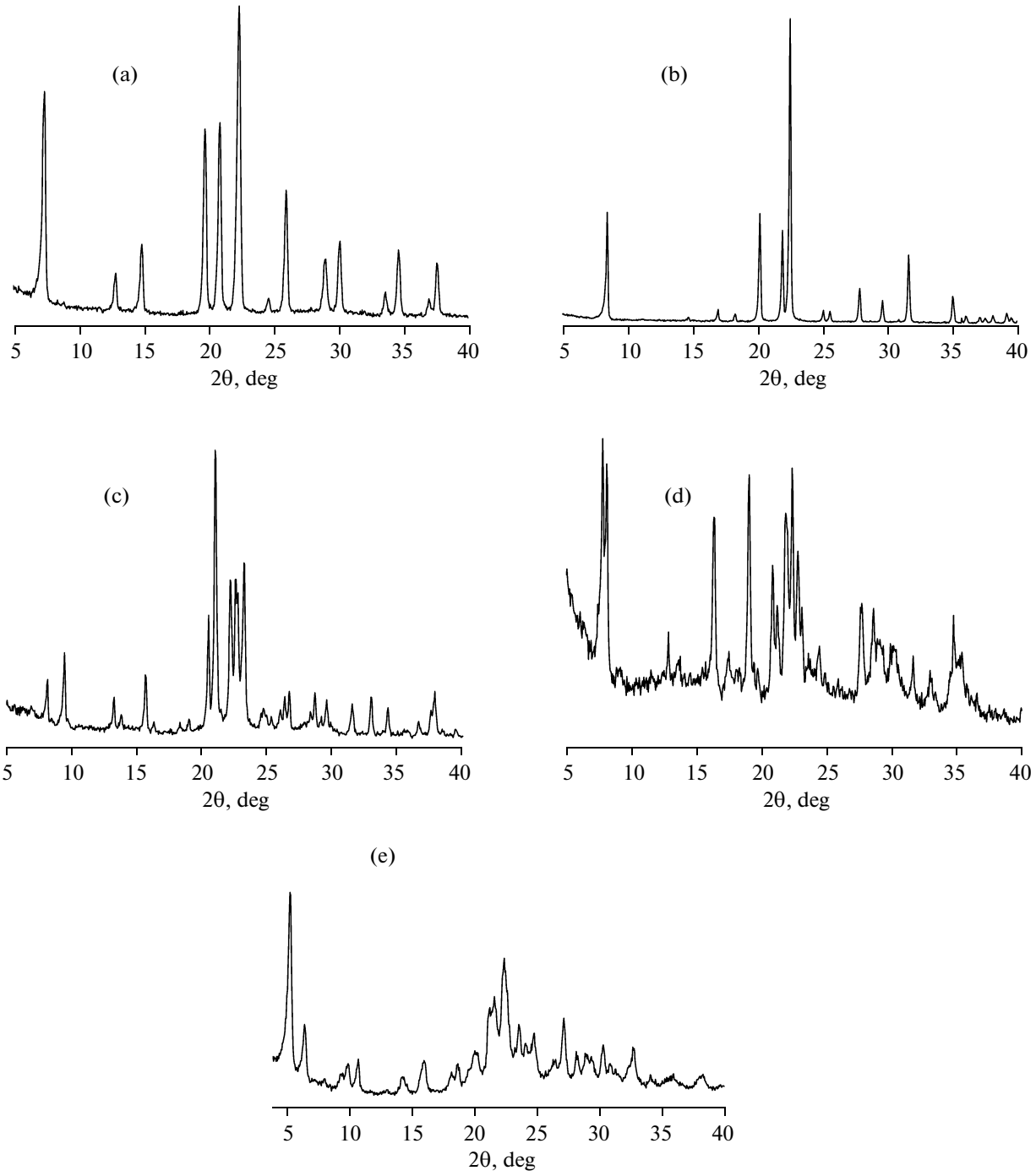


**Fig. 1.** X-ray diffraction patterns of aluminophopshate zeolites: (a) AlPO-5, (b) AlPO-31, (c) AlPO-11, (d) AlPO-36, and (e) AlPO-8.

culated using the classical Barrett–Joyner–Halenda (BJH) method [13].

## RESULTS AND DISCUSSION

According to our X-ray diffraction data (Fig. 1), the refined unit cell parameters and volume of the synthesized aluminophosphate zeolites (Table 2) are in agreement with standard data for these materials [30] within the experimental error. Note, however, that AlPO-8 (Fig. 1e) contains traces of the aluminophosphate material VPI-5, the synthetic precursor of AlPO-8 at the final heat treatment stage.

Figure 2 shows some isotherms of $N_2$ adsorption on aluminophosphate materials, and Table 3 lists calcu-

**Table 2.** Unit cell parameters for aluminophosphate zeolites

| Zeolite | $a$, Å | $b$, Å | $c$, Å | $V_{uc}$, Å$^3$ |
|---|---|---|---|---|
| AlPO-5 | 13.706 | 13.705 | 8.470 | 1377.535 |
| AlPO-31 | 20.830 | 20.830 | 4.999 | 1878.340 |
| AlPO-11 | 13.369 | 18.710 | 8.451 | 2113.882 |
| AlPO-8 | 33.162 | 14.814 | 8.376 | 4114.809 |
| AlPO-36 | 13.148 | 21.577 | 5.164 | 1464.998 |

**Table 3.** Pore structure parameters for aluminophosphate materials derived from nitrogen sorption isotherms

| Material | $S_\alpha$, m$^2$/g | $V_\mu$, cm$^3$/g | $V_s$, cm$^3$/g | $D$, nm |
|---|---|---|---|---|
| AlPO-5 | 8 | 0.111 | 0.276 | 4.0 |
| AlPO-31 | 57 | 0.038 | 0.300 | 4.0 |
| AlPO-11 | 35 | 0.051 | 0.110 | 4.1 |
| AlPO-36 | 181 | 0.061 | 0.448 | 4.0 |
| AlPO-8 | 145 | 0.078 | 0.250 | 4.1 |
| $AlPO_4$-tr | 55 | 0 | 0.106 | 4.1 |
| $AlPO_4$-q | 25 | 0 | 0.166 | 8–30 |
| $AlPO_4$-c4 | 0.1 | 0 | – | – |

lated textural characteristics of these materials. The micropore volume ($V_\mu$) and mesopore surface area ($S_\alpha$) were determined by the standard comparative method [31]. The limiting volume of the sorption space ($V_s$), which is equal to the total volume of micropores and mesopores, was determined at a maximum sorbate vapor pressure of 0.997 $P/P_0$ and the sorbate density equal to the density of the liquid phase.

It is clear from Fig. 2 that the isotherms have a noticeable capillary condensation hysteresis, which indicates that the samples have a developed mesoporous intercrystallite structure. The $AlPO_4$-c material, which has a cristobalite structure, is characterized by a very small specific surface area (Table 3) and is, therefore, unsuitable for reliable hydrogen adsorption measurements. Among the mesoporous materials, $AlPO_4$-tr, which has a tridymite structure, possesses the largest specific surface area. AlPO-36 has a more developed mesoporous structure than the other zeolites, as is indicated by the larger values of the limiting sorption space $V_s$ and mesopore surface area $S_\alpha$. This is likely due to the presence of some amount of a disperse amorphous phase in this material. The presence of the amorphous component accounts for the noticeable halo in the 10°–30° range in the X-ray diffraction pattern of this material (Fig. 1d).

Figure 3 illustrates the differential mesopore volume distribution over pore size for AlPO-5, AlPO-11, AlPO-31, $AlPO_4$-tr, and $AlPO_4$-q, as calculated by the BJH method. The values of the dominant mesopore diameter ($D$) are listed in Table 3. Clearly, the dominant pore size for AlPO-5, AlPO-31, and $AlPO_4$-tr lies in the 3–5 nm range. $AlPO_4$-q is characterized by a bimodal mesopore pore distribution over pore size. For the first and second peaks, the dominant pore diameter is 6–9 and 30 nm, respectively. The absence of finer mesopores accounts for the comparatively small specific surface area of this material.

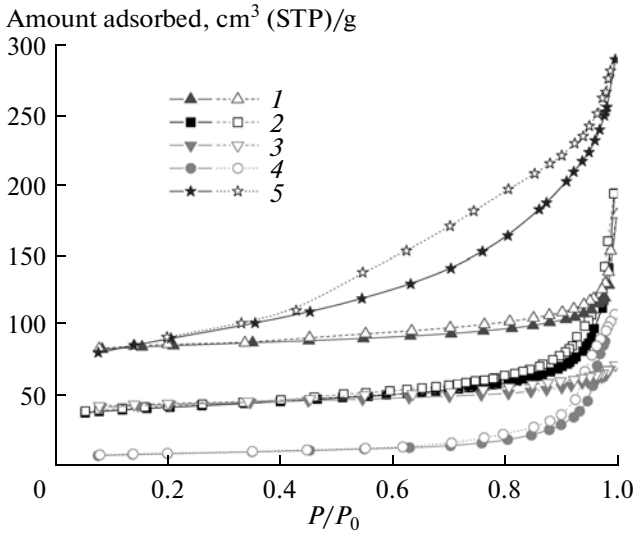


**Fig. 2.** $N_2$ adsorption (black symbols) and desorption (open symbols) isotherms at 77 K for AlPO zeolites: (*1*) AlPO-5, (*2*) AlPO-31, (*3*) AlPO-11, (*4*) $AlPO_4$-q, and (*5*) AlPO-36.

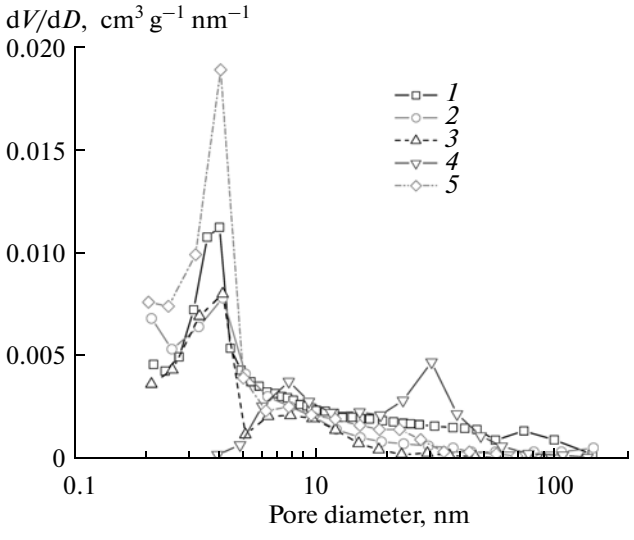


**Fig. 3.** Differential mesopore volume distribution over pore size for the AlPO zeolites (*1*) AlPO-31, (*2*) AlPO-5, (*3*) AlPO-11, (*4*) $AlPO_4$-q and (*5*) for the aluminophosphate material $AlPO_4$-tr.

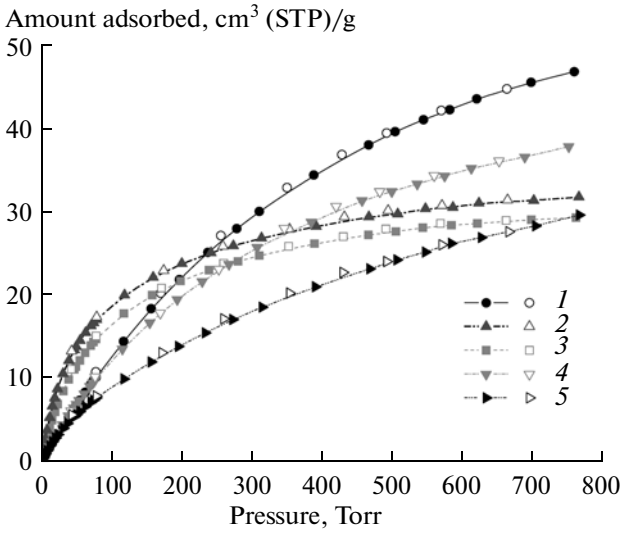


**Fig. 4.** $H_2$ adsorption (black symbols) and desorption (open symbols) isotherms at 77 K for AlPO zeolites: (*1*) AlPO-5, (*2*) AlPO-11, (*3*) AlPO-31, (*4*) AlPO-36, and (*5*) AlPO-8.

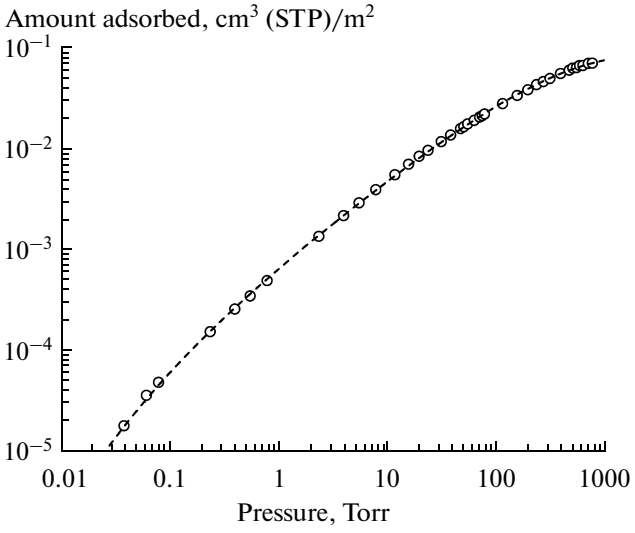


**Fig. 5.** Absolute $H_2$ adsorption isotherm at 77 K for the mesoporous aluminophosphate material $AlPO_4$-tr.

Figure 4 shows the molecular hydrogen adsorption and desorption isotherms for the AlPO zeolites at 77 K. Clearly, the isotherms are fully reversible, suggesting that there is no specific sorption on surface sites in the adsorption experiment. However, it is not absolutely impossible that there is specific sorbate–sorbent interaction detectable by more sensitive physical methods [32].

In the general case of main adsorption processes being independent, the $H_2$ adsorption isotherms at $T > T_{cr}$ for the materials containing micropores and mesopores can be represented as

$$A(P) = A^0 + S_\alpha\alpha(P) + V_\mu\beta(P, d), \qquad (1)$$

where $A^0$ is the total value of specific adsorption on Lewis and other possible surface sites [32], $S_\alpha$ is the specific mesopore surface area, $\alpha(P)$ is the absolute amount of $H_2$ adsorbed by a unit area of the mesopore surface, $V_\mu$ is the micropore volume, and $\beta(P, d)$ is the density of adsorbed hydrogen in the micropores with the diameter $d$. It follows from Eq. (1) that $A(P)$ depends on two independent variables, namely, $\alpha(P)$ and $\beta(P, d)$, which determine the sorption properties of the sorbate–sorbent pair and, for a heterogeneous surface, are usually determined experimentally.

The absolute values of the amount of hydrogen adsorbed on the mesopore surface, $\alpha(P)$, can be determined for the AlPO materials that contain no micropores, namely, $AlPO_4$-q and $AlPO_4$-tr, whose specific surface area was measured using nitrogen vapor adsorption (Table 3). The $\alpha(P)$ values thus obtained differ insignificantly, but more reliable data have been obtained for $AlPO_4$-tr, which has a larger $S_\alpha$ value. The mesopore surface area is of great significance in measuring $H_2$ adsorption at 77 K. The $\alpha(P)$ values can be satisfactorily be approximated (Fig. 5) by the relationship

$$\log\alpha(P) = -3.18367 + 0.92465\log P - 0.07282(\log P)^2 + 0.02403(\log P)^3 - 0.00856(\log P)^4, \qquad (2)$$

in which the sorbate pressure $P$ is expressed in torrs.

The density of hydrogen adsorbed on the aluminophopshate material can be estimated using Eq. (1) by representing the adsorption isotherms as

$$[A(P) - S_\alpha\alpha(P)]/V_\mu = A^0/V_\mu + \beta(P, d) = \beta^*(P, d), \qquad (3)$$

where $V_\mu$ and $S_\alpha$ are derived from nitrogen vapor adsorption data. The right-hand side of Eq. (3), $\beta^*(P, d)$, can be considered to be the effective density of adsorbed molecular hydrogen that takes into account both the effect of the adsorption potential (as a function of the size of the accessible channel, $d$) and the effect of the concentration of selective sorption sites that may occur on the surface. It can be expected that the $A^0/V_\mu$ value is not large as compared to $\beta(P, d)$; nevertheless, it should be taken into account in the general analysis of the sorption process.

Figure 6 plots the $H_2$ adsorption isotherms represented in the form of Eq. (3). The $\alpha(P)$ values for the materials were calculated via Eq. (2). It is clear from Fig. 6 that the values of the effective density $\beta^*(P, d)$ for AlPO-11 and AlPO-31 are fairly similar, but differ markedly from the $\beta^*(P, d)$ values for the zeolites AlPO-5, AlPO-36, and AlPO-8. There is every reason to believe that the sorbate density is mainly determined by the microchannel size.

The structure of the aluminophopshate zeolites was studied in a number of works and was viewed as a system of cylindrical channels with a round or ellipsoidal cross section (see, e.g., [33]), as is shown in Fig. 7. The

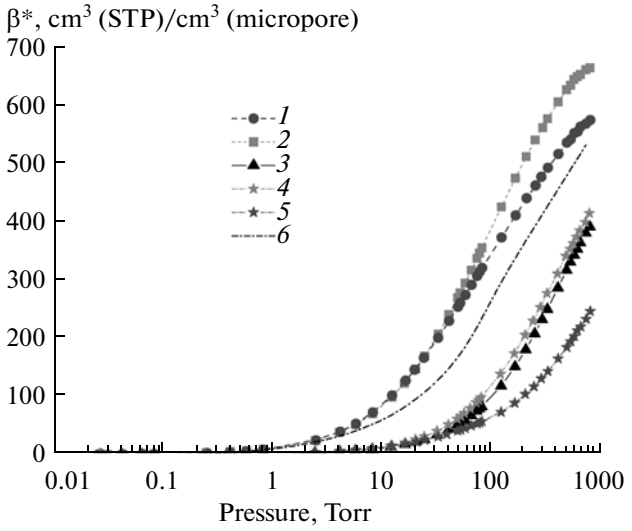


**Fig. 6.** Effective density of adsorbed $H_2$ (β*(*P*, *d*)) at 77 K for aluminophosphate zeolites: (*1*) AlPO-11, (*2*) AlPO-31, (*3*) AlPO-5, (*4*) AlPO-36, and (*5*) AlPO-8; (*6*) calculated data for $d = 0.6$ nm.

channel size is determined by the molecular probe method [26] and is derived from models of the zeolite unit cell [30, 33, 34]. On the whole, these approaches provide similar results. It can, therefore, be accepted that the micropore channel sizes presented in Fig. 7 are the true sizes of the cylindrical micropores accessible to diffusing nitrogen and hydrogen molecules. The sizes of the round and ellipsoidal channels can be approximately compared based on the principle that the cross-sectional areas of the channels are equal. According to this principle, the size of the ellipsoidal channels in AlPO-11 (major and minor axes of 0.63 and 0.39 nm) is approximately equivalent to a round channel diameter of $d \approx 0.49$ nm. The same estimate for the ellipsoidal channels in AlPO-36 (major and minor axes of 0.74 and 0.65 nm [28]) is $d \approx 0.7$ nm; for AlPO-8 (major and minor axes of 0.87 and 0.79 nm [30]), $d \approx 0.83$ nm. Thus, the dependence of the effective density of adsorbed hydrogen, β*(*P*, *d*), on the zeolite channel size *d* is quantitatively illustrated by Fig. 6.

Figure 8 presents the plot of the number of adsorbed $H_2$ molecules per unit cell of AlPO as a function of the sorbate pressure (*N*(*P*)). It is of interest to compare current *N*(*P*) values to the limiting sorption capacity ($N_{lim}$, molecule $H_2$/unit cell) corresponding to the density of liquid hydrogen at its boiling point (0.07 g/cm$^3$). The calculated $N_{lim}$ values (molecule $H_2$/unit cell) are as follows: 15.4 for AlPO-5, 8.1 for AlPO-31, 11.2 for AlPO-11, 8.55 for AlPO-36, and 32.8 for AlPO-8. Clearly, the *N*(*P*) values at 77 K in the pressure range examined do not exceed the limiting capacity of the unit cell. Obviously, at the sorption temperature 77 K, when there is no hydrogen conden-

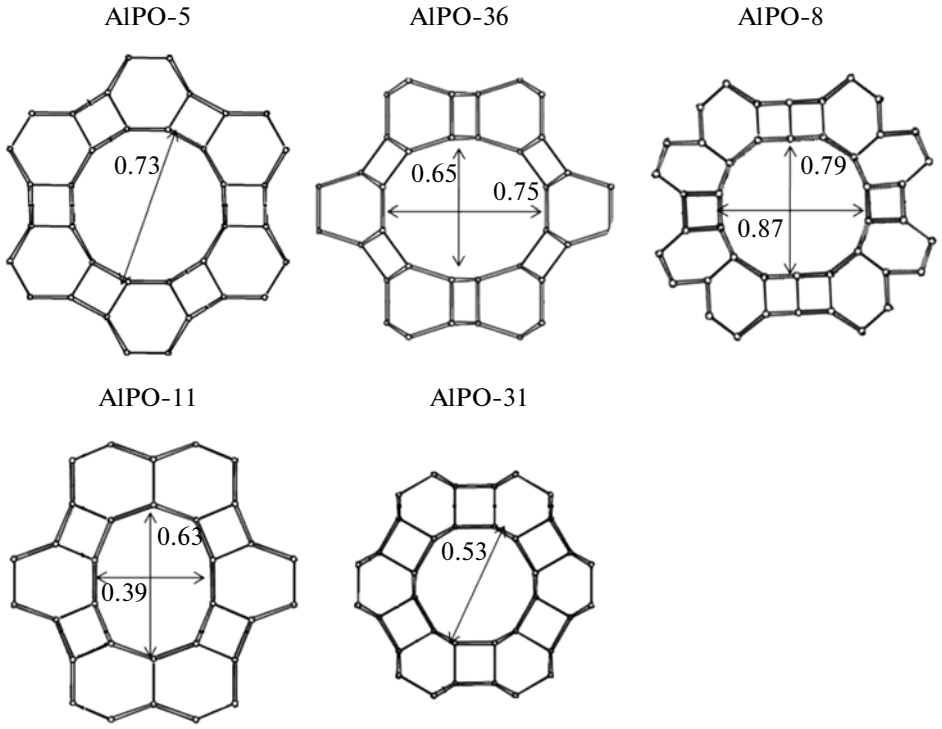


**Fig. 7.** Structure and dimensions of channels in AlPO zeolites [30, 33].

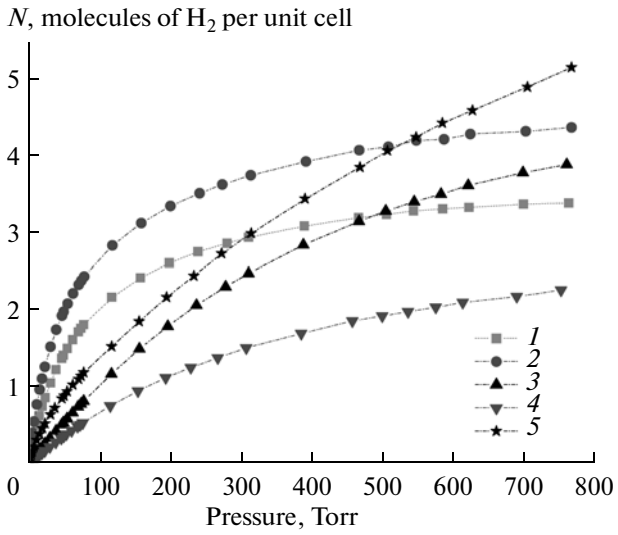


**Fig. 8.** Number of adsorbed $H_2$ molecules per unit cell as a function of pressure for AlPO zeolites: (*1*) AlPO-31, (*2*) AlPO-11, (*3*) AlPO-5, (*4*) AlPO-36, and (*5*) AlPO-8.

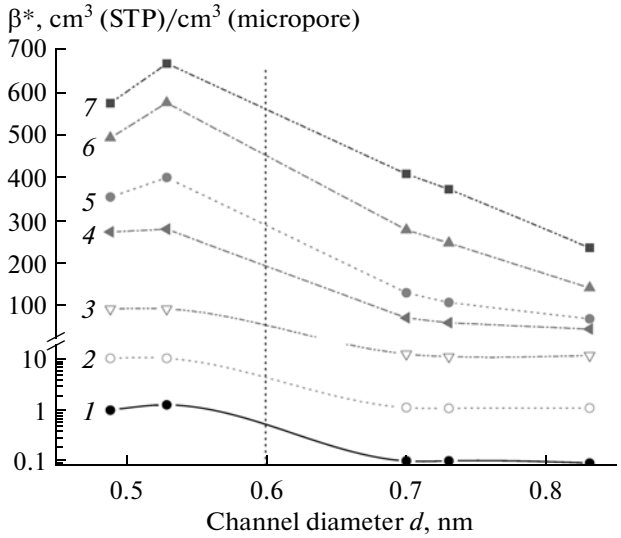


**Fig. 9.** $H_2$ adsorption isobars ($\beta^*(P, d)$) at 77 K and pressures of (*1*) 0.1, (*2*) 1, (*3*) 10, (*4*) 50, (*5*) 100, (*6*) 300, and (*7*) 700 Torr.

sation, the $N_{lim}$ value is experimentally unreachable at any pressure.

The experimental adsorption isotherms $\beta^*(P, d)$ are, in essence, analogues of local isotherms theoretically calculated for a particular model and a given pore size (so-called kernel), which are used in NLDFT calculations of pore volume distribution over pore size, including for micropores. These theoretical local 77-K $H_2$ adsorption isotherms for carbon surfaces and slitlike pores over a wide range of pore sizes are presented in, e.g., [35, 36].

It is quite obvious that it is impossible to measure a wide variety of local isotherms for aluminophosphate zeolites if the structures and chemical compositions of their unit cells are similar. In view of this, it may be reasonable and appropriate to specify the way of establishing the $\beta^*(P, d)$ correlation for intermediate $d$ values using the experimentally measured set of reference isotherms.

Figure 9 shows $H_2$ adsorption isotherms derived from experimental adsorption isotherms over the pressure range of $P = 0.1$–$700$ Torr as a function of the zeolite channel size $d$. The shape of isobars is known to provide information concerning hydrogen adsorption in pores with different diameters [36]. The isobars for the aluminophosphate zeolites, which have a distinct maximum at $d \approx 0.53$ nm, indicate that $\beta^*(P, d)$ is affected by long-range attractive forces, which strengthen as the pore diameter decreases to ~0.53 nm because of the imposition of the wall potentials of the cylindrical micropores. The finer pores are dominated by short-range repulsive forces, which reduce the sorbate density. A qualitatively similar behavior of calculated adsorption isobars is observed for the microporous carbon surface–hydrogen system at 77 K, as well as in variation of the width of model slitlike pores [36]. The quantitative distinctions between the isobars for the AlPO–$H_2$ and C–$H_2$ systems are likely due to these systems differing in molecular interaction details and in micropore shape. Figure 9 also indicates that the sensitivity of the sorbate density to the channel diameter $d$ varies with pressure. For example, $\beta^*(P, d)$ at $P < 50$ Torr is almost invariable in the $d > 0.7$ nm range, while the sorbate density at higher pressures depends significantly on the channel diameter. This experimental finding corroborates earlier theoretical calculations [36]: the higher the sorbate pressure, the stronger the effect of the wider pores present in the sample on the total amount adsorbed.

The adsorption isobars obtained in this study enable one to reliably calculate $\beta^*(P, d)$ for intermediate $d$ values (Fig. 9, dashed line for $d = 0.6$ nm) and to obtain the corresponding molecular hydrogen adsorption isotherms. Figure 6 presents a typical example of a calculated local adsorption isotherm for a hypothetical aluminophosphate zeolite with $d = 0.6$ nm.

Thus, we have determined the basic parameters characterizing the sorption interaction between molecular hydrogen and an aluminophosphate zeolite at 77 K, namely, absolute values of the amount of hydrogen adsorbed per unit area of the mesopore surface ($\alpha(P)$) and a set of local isotherms for zeolites with a known channel size ($\beta^*(P, d)$). Use of these parameters could improve experiment-based methods for calculating the micropore volume distribution over pore size $d$, including for zeolites whose channels accommodate the active component of a catalyst.

## REFERENCES


1. Kharas, K.C.C., Liu, Di-Jia., and Robota, H.J., *Catal. Today*, 1995, vol. 26, no. 2, p. 129.
2. Moretti, G., Dossi, C., Fusi, A., Recchia, S., and Psaro, R., *Appl. Catal., B*, 1999, vol. 20, no. 1, p. 67.
3. Groothaert, M.H., Lievens, K., Leeman, H., Weckhuysen, B.M., and Schoonheydt, R.A., *J. Catal.*, 2003, vol. 220, no. 2, p. 500.
4. Petunchi, J.O., Sill, G., and Hall, W.K., *Appl. Catal., B,* 1993, vol. 2, no. 4, p. 303.
5. Yashnik, S.A., Ismagilov, Z.R., and Anufrienko, V.F., *Catal. Today*, 2005, vol. 110, nos. 3–4, p. 310.
6. Li, L. and Guan, N., *Microporous Mesoporous Mater.*, 2009, vol. 117, nos. 1–2, p. 450.
7. Arishtirova, K., Dimitrov, Chr., Dyrek, K., Hallmeier, K.-Hz., Popova, Z., and Witkowski, S., *Appl. Catal., A*, 1992, vol. 81, no. 1, p. 15.
8. Hedge, S.G., Ratnasamy, P., Kustov, L.M., and Kazansky, V.B., *Appl. Spectrosc.*, 1988, vol. 8, no. 2, p. 137.
9. Yingxu Wei, Gongwei Wang, Zhongmin Liu, Peng Xie, Yanli He, and Lei Xu, *Catal. Lett.*, 2003, vol. 91, nos. 1–2, p. 35.
10. Wei, W., Moulijn, J.A., and Mul, G., *Microporous Mesoporous Mater.*, 2008, vol. 112, nos. 1–3, p. 193.
11. Krivoruchko, O.P., Larina, T.V., Shutilov, R.A., Gavrilov, V.Yu., Yashnik, S.A., Sazonov, V.A., Molina, I.Yu., and Ismagilov, Z.R., *Appl. Catal., B,* 2011, vol. 103, nos. 1–2, p. 1.
12. Gavrilov, V.Yu., Krivoruchko, O.P., Larina, T.V., Molina, I.Yu., and Shutilov, R.A., *Kinet. Catal.,* 2010, vol. 51, no. 1, p. 88.
13. Barrett, E.P., Joyner, L.G., and Halenda, P.P., *J. Am. Chem. Soc.*, 1951, vol. 73, no. 1, p. 373.
14. Dollimore, D. and Heal, G.R., *J. Appl. Chem.*, 1964, vol. 14, p. 109.
15. Broekhoff, J.C.P. and de Boer, J.H., *J. Catal.*, 1967, vol. 9, no. 1, p. 8.
16. Horvath, G. and Kavazoe, K., *J. Chem. Eng. Jpn.*, 1983, vol. 16, p. 470.
17. Lastoskie, Ch.M. and Gubbins, K.E., *Stud. Surf. Sci. Catal.*, 2000, vol. 128, p. 41.
18. Ustinov, E.A. and Do, D.D., *Langmuir*, 2004, vol. 20, no. 9, p. 3791.
19. Neimark, A.V., Lin, Y., Ravikovitch, P.I., and Thommes, M., *Carbon*, 2009, vol. 47, no. 7, p. 1617.
20. Sweatman, M.B. and Quirke, N., *J. Phys. Chem. B*, 2001, vol. 105, no. 7, p. 1403.
21. Jagiello, J. and Thommes, M., *Carbon*, 2004, vol. 42, no. 7, p. 1227.
22. Gavrilov, V.Yu., *Kinet. Katal.*, 1995, vol. 36, no. 4, p. 631.
23. Jagiello, J. and Bets, W., *Microporous Mesoporous Mater.*, 2008, vol. 108, nos. 1–3, p. 117.
24. Gavrilov, V.Yu. and Zakharov, R.S., *Kinet. Catal.*, 2010, vol. 51, no. 4, p. 609.
25. Gavrilov, V.Yu., *Kinet. Katal.,* 1995, vol. 36, no. 5, p. 787.
26. Flanigen, E.M., Lok, B.M., Patton, R.L., and Wilson, S.T., *Pure Appl. Chem.*, 1986, vol. 58, no. 10, p. 1351.
27. US Patent 4310440, 1982.
28. Hassan Zahedi-Niaki, M., Joshi Praphulla, N., and Kaliaguine Serge, *Chem. Commun.*, 1996, vol. 11, no. 11, p. 1373.
29. Tsybulya, S.V., Cherepanova, S.V., and Solov'eva, L.P., *Zh. Strukt. Khim.*, 1996, vol. 37, no. 2, p. 379.
30. *Atlas of Zeolite Framework Types*, Baerlocher, Ch., McCusker, L.B., and Olson, D.H., Eds., Amsterdam: Elsevier, 2007.
31. Karnaukhov, A.P., *Adsorbtsiya. Tekstura dispersnykh i poristykh materialov* (Adsorption and Texture of Disperse and Porous Materials), Novosibirsk: Nauka, 1999.
32. Kazansky, V.B., *J. Catal.*, 2003, vol. 216, nos. 1–2, p. 192.
33. Bennett, J.M. and Kirchner, R.M., *Appl. Spectrosc.*, 1992, vol. 12, no. 4, p. 338.
34. Li, I.L. and Tang, Z.K., *Appl. Phys. Lett.*, 2002, vol. 80, no. 25, p. 4822.
35. Jagiello, J., Anson, A., and Martínez, M.T., *J. Phys. Chem. B*, 2006, vol. 110, no. 10, p. 4531.
36. Gavrilov, V.Yu. and Ustinov, E.A., *Kinet. Catal.*, 2011, vol. 52, no. 3, p. 459.